THE ASTROPHYSICAL JOURNAL, 423:334–343, 1994 March 1

IUE SPECTRA AND OPTICAL IMAGING OF THE OXYGEN-RICH SUPERNOVA REMNANT N132D

WILLIAM P. BLAIR,[1,2,3] JOHN C. RAYMOND,[2,4] AND KNOX S. LONG[3,5]
Received 1993 April 12; accepted 1993 September 13

ABSTRACT

We present new optical CCD/interference filter imagery and *IUE* spectroscopy for the oxygen-rich supernova remnant N132D in the Large Magellanic Cloud. The optical images show a wealth of structure, and comparison with an archival *Einstein* HRI X-ray image shows that a few optical features have X-ray counterparts, but in general there is little correlation between X-ray and optical features. The *IUE* spectra at two positions show strong lines of carbon and oxygen, with lines of neon, magnesium, silicon, and helium also present and variable in relative intensities. We use optical data for N132D from Dopita & Tuohy (1984) with our UV observations to compare with shock models (both with and without thermal conduction) and X-ray photoionization model calculations. While none of the model fits is entirely satisfactory, the generally weak UV emission relative to optical disagrees with the general character of shock model predictions and indicates that photoionization is the dominant excitation mechanism for the UV/optical emission. This conclusion is similar to what was found for E0102−7219, the oxygen-rich remnant in the Small Magellanic Cloud. We derive rough abundances for the emitting material in N132D, compare to stellar nucleosynthesis models, and discuss the implications for its precursor. A precursor near 20 $M_\odot$ is consistent with the data.

Subject headings: ISM: individual (N132D) — supernova remnants — ultraviolet: interstellar

1. INTRODUCTION

N132D is a young supernova remnant (SNR) located in the bar of the Large Magellanic Cloud (LMC). The optical emission was first cataloged by Henize (1956) as a rather faint nebulosity in a very dense star field. Radio observations by Westerlund & Mathewson (1966) showed a nonthermal spectrum for the object and suggested the SNR identification. Optical spectroscopy (Danziger & Dennefeld 1976; Lasker 1978, 1980) quickly showed that the object was peculiar, with strong and variable oxygen and sulfur emission lines and both high- and low-velocity components. A faint, nearly circular disk with diameter ~80″ (19.4 pc assuming the LMC is at a distance of 50 kpc—see Eastman & Kirshner 1989) encloses brighter knots of emission which show peculiar line ratios and high velocities. The disk, which Lasker describes as diffuse, can be seen in both [O III] and Hα. The knots show a velocity range of at least ±2200 km s^{-1} and may be distributed in an annular structure with diameter ~6 pc tilted ~45° to the line of sight, although recent Fabry-Perot data may call this interpretation into dispute (J. Morse, private communication). The kinematic age for the object is thus about 1300 yr. Dopita & Tuohy (1984) produced a "global" spectrum of the high-velocity oxygen emission from N132D showing only lines of oxygen and neon in the 3400–5200 Å range. The lower velocity knots emit at Hα and [S II]. Lasker & Golimowski (1991) recently reported a negative search for any high-velocity sulfur emission from N132D. A larger (~5′ diameter), partial ring of very faint [O III] emission may be interstellar material ionized by the UV pulse from the supernova explosion.

These characteristics clearly place N132D in the class of oxygen-rich SNRs, which includes such objects as Cas A and G292.0+1.8 in our Galaxy (Chevalier & Kirshner 1978, 1979; Goss et al. 1979; Murdin & Clark 1979), E0102.2−7219 in the SMC (Dopita, Tuohy, & Mathewson 1981; Blair et al. 1989), 0540−69.3 in the LMC (Mathewson et al. 1980; Kirshner et al. 1989), and the powerful young SNR in the irregular galaxy NGC 4449 (Blair, Kirshner, & Winkler 1983). More recently, the remnant of SN 1957D in M83 has also been recovered optically, showing only lines of oxygen in its spectrum (Long, Blair, & Krzeminski 1989), although this emission has faded over a several year timescale (Long, Winkler, & Blair 1992). Some knots dominated by oxygen emission have also been identified in the galactic remnant Puppis A (Winkler & Kirshner 1985), although this SNR is thought to be considerably older than the other members of the class.

N132D was found to be the brightest extended soft X-ray source in the LMC (Long, Helfand, & Grabelsky 1981; Mathewson et al. 1983), with a luminosity of L_x(0.15–4.5 keV) = 8.3 × 10^{37} ergs s^{-1}. Clark et al. (1982) used the *Einstein* Solid State Spectrometer to demonstrate the X-ray emission was thermal in nature. More recently, Hughes (1987) has analyzed the distribution of the X-ray emission using *Einstein* HRI data and builds a consistent model assuming the explosion occurred in a cavity blown by the precursor star. *Einstein* Focal Plane Crystal Spectrometer data (Canizares 1990; Hwang et al. 1992, 1993) show very strong O VIII 0.645 keV emission from the central regions, consistent with the oxygen-rich designation. Hwang et al. (1993) have performed a detailed analysis of all of the *Einstein* data and develop a "single temperature, single ionization timescale nonequilibrium ionization model" yielding T_X = 8.4 × 10^6 K and an "ionization age" (given as the invariant quantity $n_e t$) of 6.1 × 10^3 cm^{-3} yr (cf. Hamilton, Sarazin, & Chevalier 1983).

[1] Department of Physics and Astronomy, Johns Hopkins University, 34th & Charles Streets, Baltimore, MD 21218.
[2] Guest Observer with the *International Ultraviolet Explorer* satellite, which is jointly operated by the US National Aeronautics and Space Administration, the Science Research Council of the UK, and the European Space Agency.
[3] Guest Observer, Las Campanas Observatory, operated by the Carnegie Institution of Washington.
[4] Center for Astrophysics, 60 Garden Street, Cambridge, MA 02138.
[5] Space Telescope Science Institute, 3700 San Martin Drive, Baltimore, MD 21218.

Objects with inferred large overabundances of such elements as oxygen, neon, sulfur, etc., are thought to represent the explosions of massive (Population I) stars. Nuclear burning in the progenitor stars had progressed to or perhaps even beyond the oxygen-burning stage when the SN explosion took place. With the exception of Puppis A, the oxygen-rich SNRs are all young ($\leq$2500 yr), show high-velocity material ($\Delta v \geq 2000$ km s^{-1}, and contain some optical knots or filaments whose spectra are dominated by oxygen emission lines. Since the X-ray emissivity depends on n_e^2 and is also a function of heavy element abundances (cf. Raymond & Smith 1977; Long, Dopita, & Tuohy 1982), these young, metal-rich SNRs also tend to be strong soft X-ray sources. N132D is no exception in this regard.

UV spectra of oxygen-rich SNRs are crucial because some important elements such as carbon, silicon, and magnesium have no strong lines in the optical and their abundances are unconstrained by optical spectra. The ultraviolet region contains strong lines of these elements as well as oxygen and neon. Unfortunately, most oxygen-rich remnants are too faint or too reddened to be detected by *IUE* or *HST*. The SNR in NGC 4449 was observed by Blair et al. (1984), but only the O III] λ1665 line was seen against the bright H II region background. The SMC remnant E0102.2−7219 (hereinafter E0102) was detected with *IUE* by Blair et al. (1989) in an investigation very similar to the one reported here for N132D. One of the conclusions of that paper was that X-ray photoionization of the ejecta was an important excitation mechanism.

In this paper we report new optical CCD/interference filter imagery of N132D and both long- and short-wavelength *IUE* ultraviolet spectra at two positions in the enriched optical knots. The CCD images show the optical extent of the object more clearly than previous work and a comparison with the *Einstein* HRI image is made. The *IUE* spectra show lines of carbon, oxygen, neon, magnesium, silicon, and helium with substantial variations in relative line intensities between the two positions. The observations are described in the following section and discussed in § 3.

2. OBSERVATIONS AND REDUCTIONS

2.1. *Optical Imagery*

We used a TI 800 × 800 CCD with a focal reducer on the 2.5 m du Pont telescope at Las Campanas Observatory to obtain images of N132D in 1987 November. The focal reducer (the CHUEI—similar to the PFUEI described by Gunn & Westphal 1981) compressed the f/7.5 telescope beam down to f/2.7, yielding a scale of 0.″41 pixel^{-1} on the CCD and providing a field 5.′3 square. The following interference filters and exposure times were used: an Hα filter (λ_0 = 6565 Å, FWHM = 30 Å; 1000 s) a [S II] filter (λ_0 = 6737 Å, FWHM = 57 Å; 1000 s), a red continuum filter (λ_0 = 6100 Å, FWHM = 130 Å; 500 s), and an [O III] filter (λ_0 = 5027 Å, FWHM = 53 Å; 1500 s). The effective seeing was ~2.″5 (FWHM) for these images but transparency was excellent. Spectrophotometric standard stars from the list of Stone & Baldwin (1983) were observed through the filters each night.

The CCD images were bias-subtracted and divided by normalized dome flat fields to take out pixel-to-pixel variations in the CCD. In Figure 1 (Plate 6) we show 3′ portions of these frames centered on N132D. Because much of the emission is knotty or nearly stellar in appearance or exceedingly faint, the true character and extent of the SNR emission is not obvious in these images. Hence, these images have been processed further by subtracting sky background, aligning and scaling the continuum image to each emission line image, and then subtracting. Because of seeing variations from frame to frame and slightly different distortions in the filters, as well as color differences in the stars, this procedure does not completely remove stars. However, this simple procedure does reduce much of the clutter and draws the eye to real SNR emission even in the crowded star fields (see Blair, Long, & Vancura 1991). Figures 2*a*, 2*b*, and 2*c* (Plate 7) show the subtracted versions of the emission line images seen in Figure 1*a*, 1*b*, and 1*c*, highlighting the faintest emission.

In order to compare the optical morphology with the X-ray gas, we have obtained an *Einstein* HRI image of N132D from the *Einstein* database. This exposure was H4286, obtained with a 8590 s exposure on 1979 day 199. The X-ray data were aligned with the optical images and smoothed with a Gaussian filter of σ = 2.5 pixels (=2.″5). The relative astrometry should be accurate to within ~4″. The resulting image is shown in Figure 2*d* to the same scale as the subtracted optical images. A comparison of these images will be made below.

2.2. *IUE Spectroscopy*

Long-exposure SWP and LWP spectra were obtained with *IUE* at each of two positions in N132D, as summarized in Table 1. Position 1 was centered at R.A.(1950) 05^{h}26^{m}02^s.26, Decl.(1950) −69°38′12.″8, on a region with relatively strong [O III] emission (Lasker's 1978 knot 3). Position 2 was centered at R.A.(1950) 05^{h}25^{m}26^s.40, Decl.(1950) −69°40′40.″8, about 23″ west-northwest of position 1 on a region of relatively strong [S II] and Hα emission (Lasker's 1978 knot 6 and the west end of arc 4). The positions of the *IUE* large aperture are shown in Figure 1*a* to scale and in the proper orientation. The *IUE* large aperture was positioned by blind offsetting from SAO 249273 (V = 8.6) to the positions above. Astrometry was done both with a measuring engine at the Center for Astrophysics and with the *HST* Guide Star catalog; the results are consistent at the $\leq$2″ level. The blind offset maneuver was only ~3′, so the offset error should have been less than 1″.

The exposure times were maximized by combining low-background ESA/US1 *IUE* shifts. Each exposure was set up and begun at the Villafranca tracking station in Spain and then handed over to NASA/GSFC where the exposure was completed and read out. Serendipitous exposures were made during each primary exposure with the "other" *IUE* camera (i.e., whichever one was not exposing on the SNR). These exposures provide information on the general *IUE* background in regions directly adjacent to the SNR (~1.′1 away). The results of these exposures are also summarized in Table 1. The positions for the serendipitous exposures were fixed by the aperture orientation and the known separation of long- and short-wavelength cameras' large apertures.

We have extracted the spectra from the line-by-line data files on the guest observer tapes in order to optimize the signal-to-noise ratio of the resulting spectra. These reductions were performed at Johns Hopkins using an IRAF[6]–based *IUE* reduction package that we have developed.

(The 1987 data were also reduced at the GSFC RDAF using IDL; the results from the two reductions were essentially identical.) Because of the long exposures and the background char-

[6] IRAF is distributed by the National Optical Astronomy Observatories, which is operated by the Association of Universities for Research in Astronomy, Inc. (AURA), under cooperative agreement with the National Science Foundation.

PLATE 6

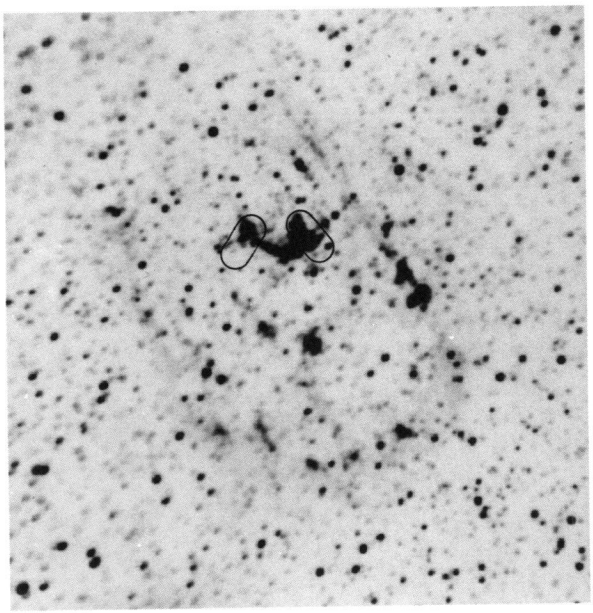

FIG. 1*a*

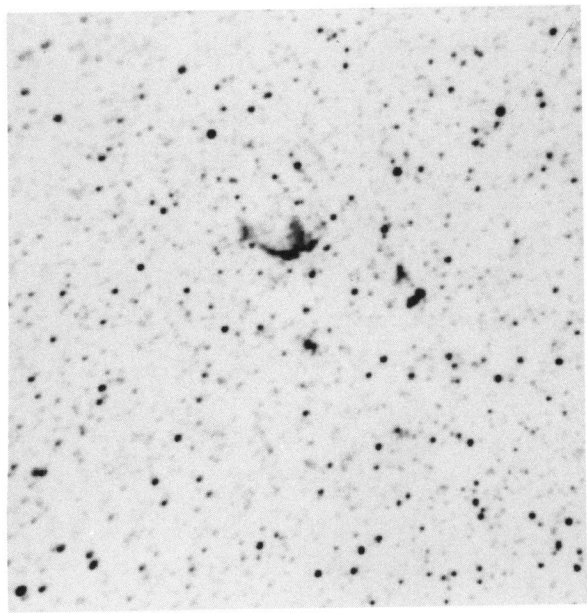

FIG. 1*b*

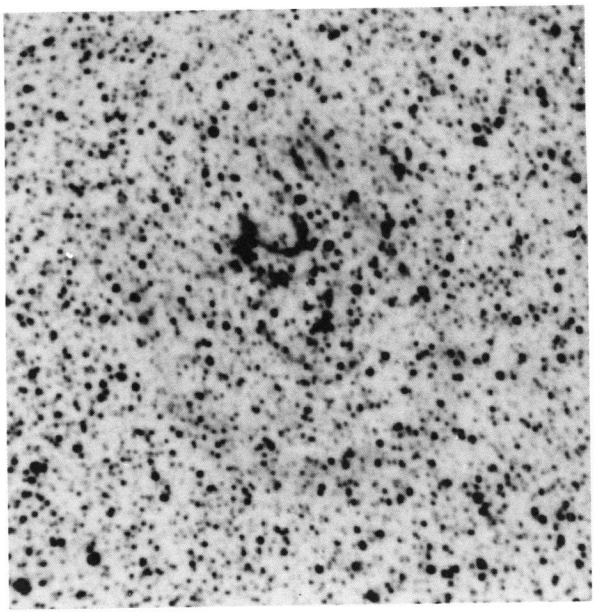

FIG. 1*c*

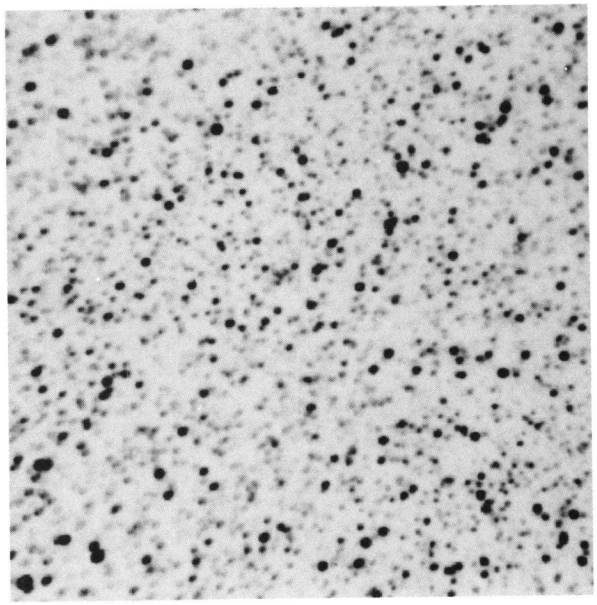

FIG. 1*d*

FIG. 1.—CCD interference filter images of N132D. (*a*) Hα; (*b*) [S II]; (*c*) [O III]; (*d*) 6100 Å continuum. North is up and east to the left. The region shown is 3′ on a side. The *IUE* positions are indicated on panel *a*.

BLAIR, RAYMOND, & LONG (see 423, 335)

FIG. 2*a*

FIG. 2*b*

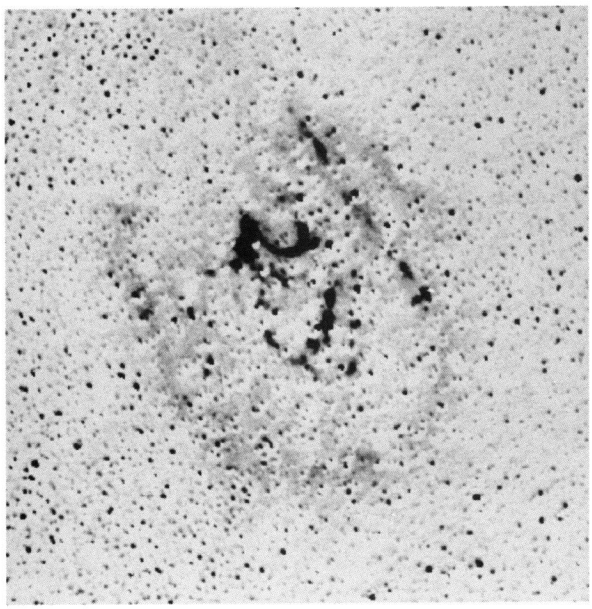

FIG. 2*c*

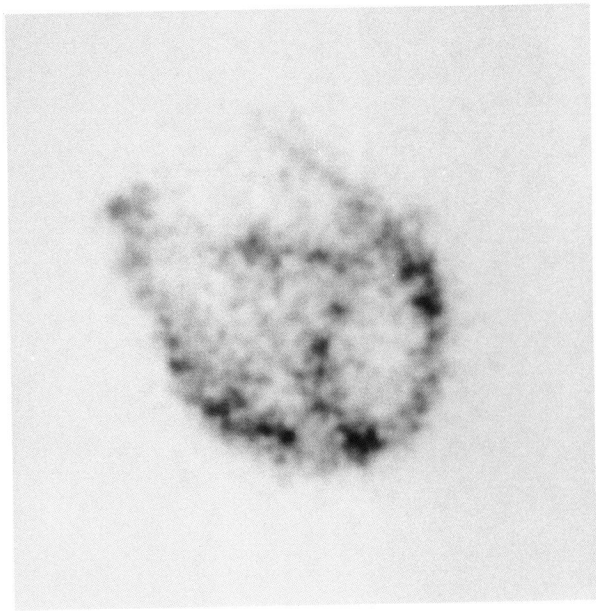

FIG. 2*d*

FIG. 2.—CCD interference filter images of N132D after scaling and subtracting the continuum image. Panels *a*, *b*, and *c* are as in Fig. 1. Panel *d* shows the aligned *Einstein* HRI image in gray-tone format for comparison.

TABLE 1

IUE OBSERVATIONS OF N132D REGION

Image Number	Date	Program ID	Exposure (minutes)	PA (°)	Comments
SWP 31578.....	1987 Aug 16	SRJWB	685	−226	SNR Pos. 1
LWP 11410	1987 Aug 16	SRJWB	325	−226	Serendipitous during SWP 31578 SSE of SNR position V. Ft. Continuum >2400 Å
LWP 12671	1988 Feb 15	SRJWB	730	−43.4	SNR Pos. 1
SWP 32929.....	1988 Feb 15	SRJWB	665	−43.4	Serendipitous during LWP 12671 SSE of SNR position Blank field
SWP 36194.....	1989 May 5	NOKWB	910	+36.4	SNR Pos. 2
LWP 15456	1989 May 5	NOKWB	850	+36.4	Serendipitous during SWP 36194 ENE of SNR position Two or more faint stars in aperture
LWP 15463	1989 May 6	NOKWB	865	+36.7	SNR Pos. 2
SWP 36200.....	1989 May 6	NOKWB	455	+36.7	Serendipitous during LWP 15463 WSW of SNR position Possible faint star in aperture

acteristics of the *IUE* cameras, the background levels in these exposures are very high, typically in the 150–180 DN range. However, because the emission is mainly in emission lines and because the emission is spatially extended, reasonable spectra can be obtained from careful extractions.

In Figure 3 (Plate 8) we show the two-dimensional data to provide an indication of the spatial extent of the emission in the various spectra. The data in this figure have had reseaux and particle events removed from the region in and near the spectra. A distinct and apparently diffuse continuum is seen in some of the spectra (especially position 2), although some evidence of faint stellar contamination is also present. There is some evidence from inspection of Figure 3 that this diffuse emission has about the same spatial extent as the emission lines (or perhaps slightly larger). Also, inspection of the serendipitous exposures shows that, while faint stars were sometimes present at these positions, *no comparable diffuse continuum appears to be present*, with an upper limit about $\frac{1}{4}$ that of the level seen at position 2. The star field throughout this region of the LMC is very dense, but it would take an unlikely coincidence to evenly space stars of nearly the same spectral type throughout the aperture to produce an apparent diffuse continuum. We tentatively conclude that the diffuse emission seen in Figure 3 is intrinsic to N132D. A similar effect was seen in the *IUE* data for E0102 in the SMC (Blair et al. 1989).

The SWP and LWP large apertures are centered at line 55 and extend for ±15 lines in the ELBL (extended line-by-line) data. In all cases, the relatively clean edges of the emission in the spatial direction are not due to the edge of the aperture. Using cross cuts in the spatial dimension at the positions of apparent emission lines, the extent of the SNR emission was measured and line numbers for each extraction chosen. In all four spectra, reasonably bright emission is seen above the background in 12–15 lines in the spatial dimension, corresponding to ~8″–10″, which is consistent with the emission seen at each position in our images.

We extracted the lines containing SNR emission into one-dimensional spectra and extracted representative backgrounds from lines directly adjoining the large aperture. The backgrounds were averaged together, scaled (if necessary) to the same number of lines as the SNR emission, smoothed, and subtracted from the SNR data. We then applied the inverse sensitivity curves of Bohlin (1986) to convert the data to observed fluxes. The resulting spectra are shown in Figure 4 after smoothing over 3 pixels (using the "splot" task in IRAF).

The centroids, widths, and integrated fluxes for all obvious emission lines have been measured using the "splot" task in IRAF. The results of these measurements as well as line identifications are shown in Table 2. Many of the features are distinctly non-Gaussian, so the widths provide only an

TABLE 2

OBSERVED AND REDDENING CORRECTED UV EMISSION-LINE INTENSITIES IN N132D

Ion	λ_{rest} (Å)	λ_{meas} (Å)	$F(\lambda)$[a]	FWHM (Å)
Position 1				
O IV]	1402.	1400.1	1.16E-13	11.3
C IV	1549.	1547.0	1.43E-13	11.7
He II	1640.	1640.4	4.28E-14	11.9
O III]	1665.	1664.6	1.01E-13	14.9
Si III]	1885.	1890.	<1.24E-14	...
[C III]	1907.	1907.1	7.61E-14	10.5
C II]	2326.	2331.4	1.25E-13	9.7
[Ne IV]	2425.	2426.7	4.33E-14	13.9
[O II]	2470.	2473.8	4.04E-14	14.6
Mg II	2798.	2799.7	3.63E-14	25.8
Position 2				
O IV] + Si IV	1395., 1402.	1399.0	5.33E-14	14.9
C IV	1549.	1548.5	1.25E-13	10.5
He II	1640.	1640.0	7.47E-14	11.8
O III]	1665.	1665.1	3.79E-14	8.9
Si III]	1885.	1884.1	4.32E-14	11.9
[C III]	1907.	1907.6	1.04E-13	10.5
C II]	2326.	2329.8	1.63E-13	11.6
[Ne IV]	2425.	2429.0	4.89E-14	16.4
[O II]	2470.	2472.5	4.91E-14	11.5
Mg II	2798.	2808.6	1.57E-14	12.4

[a] Integrated fluxes in units of ergs cm^{-2} s^{-1}.

PLATE 8

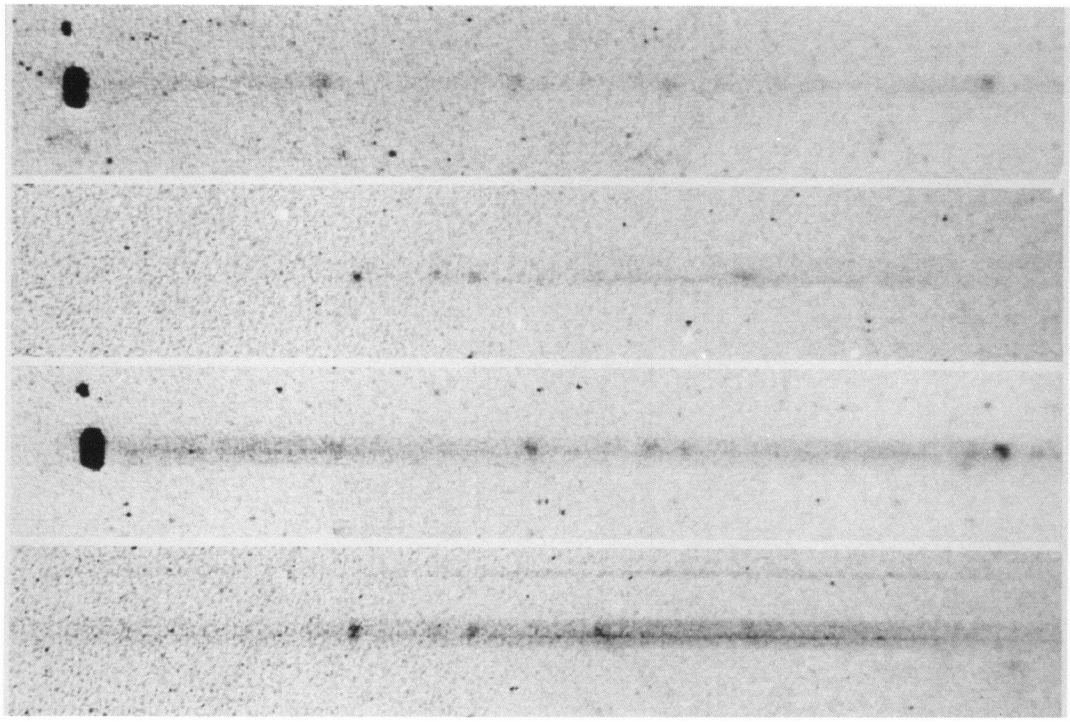

FIG. 3.—Two-dimensional *IUE* spectra for two positions in N132D. The top two panels show data for position 1, and the bottom two panels show data for position 2 (SWP on top and LWP on the bottom in each case).

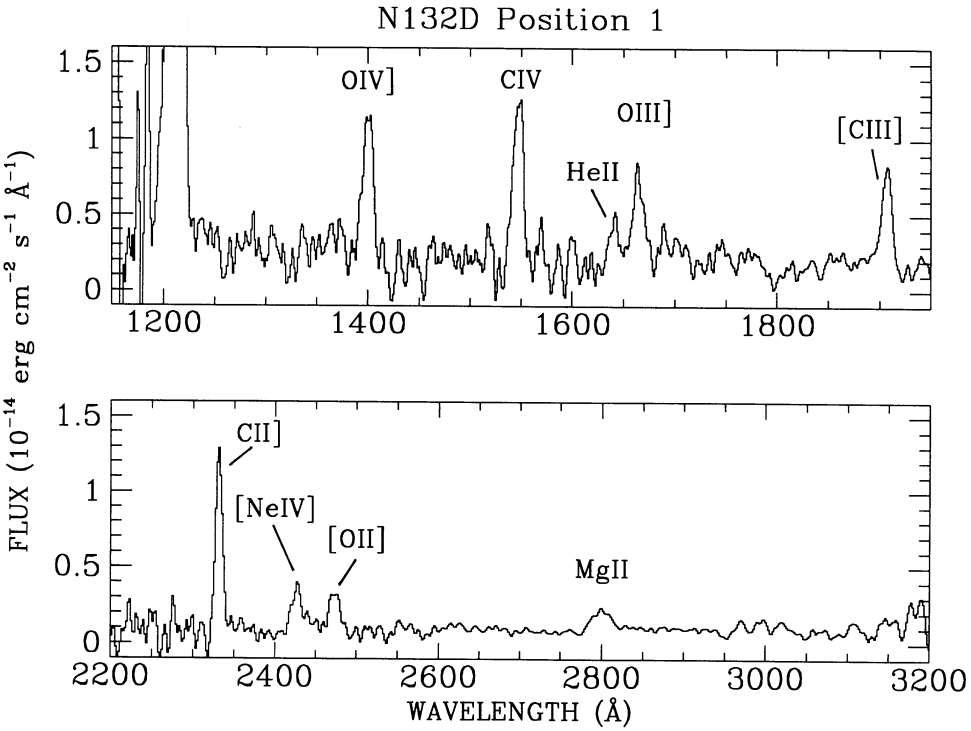

FIG. 4*a*

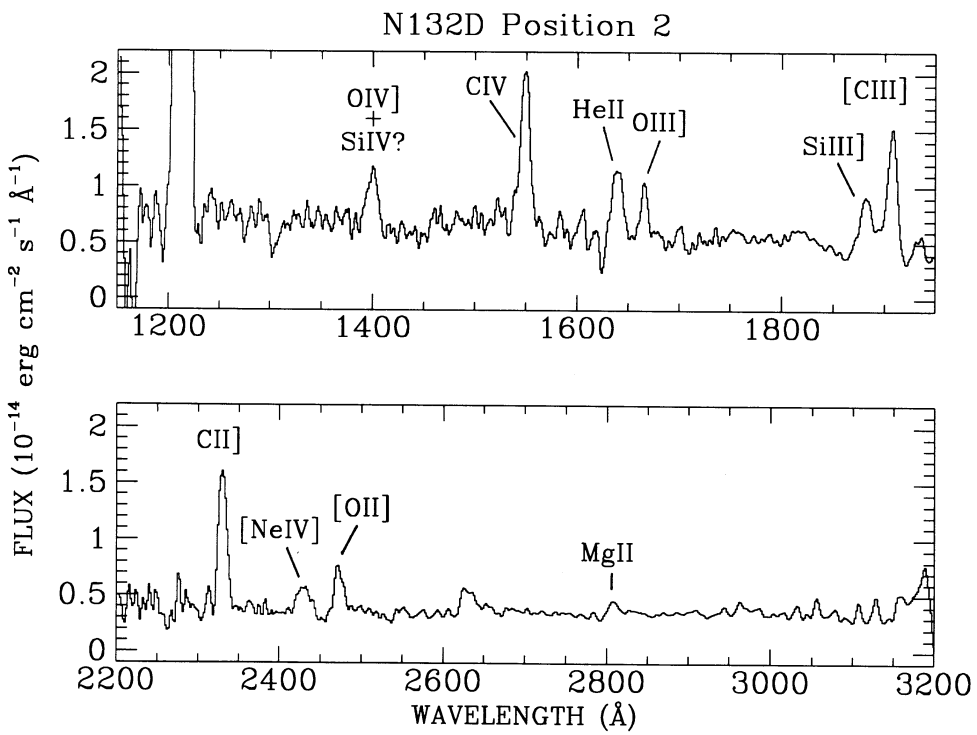

FIG. 4*b*

FIG. 4.—Extracted *IUE* spectra for N132D. Fig. 4*a* shows the data for position 1, and Fig. 4*b* shows the data for position 2.

approximation of the true widths of the features. An extended source filling the *IUE* large aperture typically produces features with ~10 Å FWHM. The narrowest well-detected features are basically consistent with this value, although these widths could also be due to smaller spatial features with some velocity broadening. A few features appear anomalously broad in comparison with most of the lines, the best example of which is Mg II λ2798 in the position 1 spectrum. The FWHM of this feature corresponds to a velocity of nearly 2800 km s^{-1}, or about 50% larger than other well-detected lines such as C IV λ1549. Interestingly, the Mg II feature in the position 2 data also appears anomalous, being shifted considerably to the red and showing an apparent absorption near the rest wavelength. Since a faint star contaminates the position 2 spectrum, caution is advised in the interpretation of this feature, but inspection of Figure 3 makes it clear that Mg II emission from the SNR is definitely present. Some of the fainter lines may be adversely affected by noise, and the well-known hot pixels in the SWP camera at ~1664 Å have been removed (to first order) from O III] λ1665 line. A particle "hit" nearly tangential to the camera face plate is evident in the position 2 spectrum near 2625 Å and has not been removed.

In general, the emission lines are too faint to allow a successful search for spatial variations within the *IUE* large aperture. At position 1, for instance, comparison against the optical images shows that two relatively bright and chemically distinct knots are included within the aperture, but no spatial variations are detected in the *IUE* spectrum. At position 2, there is some possible variation in the relative strength of Si III] λ1885 across the aperture, although there is some possibility of contamination by one or more particle events. From our inspection of the data, the feature looks real and we tentatively ascribe it to Si III].

The spectra at the two positions basically show the same lines, but the relative intensities vary considerably. Lines of He, C, O, Ne, and Mg dominate the spectra at both positions. No N lines have been detected at either position. Assuming the Si III] line at 1885 Å is correctly identified in the position 2 spectrum, it seems likely that Si IV may contribute to the feature at 1400 Å in this spectrum. In the position 1 spectrum, however, only an upper limit on the Si III] line is available; since O III] λ1665 is stronger at this position (as is the 1400 Å feature itself), we assume that the 1400 Å feature in the position 1 spectrum is dominated by O IV]. He II λ1640 is present at both positions, but stronger at position 2. C II] λ2326 is strong at both positions but there is no evidence for C II λ1335. The 1907 Å feature is a well-known C^{++} doublet consisting of a forbidden line at 1907 Å and an intercombination line at 1909 Å. Both from the measured wavelengths of this feature in the spectra and from the physical conditions expected in the emitting material of N132D, we assume that the forbidden component dominates.

We make no explicit attempt to correct these lines for reddening effects. The extinction to N132D is not well determined; Lasker (1978) measured a Balmer decrement to the faint halo of N132D which is consistent with a moderate amount of reddening, $E(B-V) \leq 0.15$. Hwang et al. (1993) obtain a best-fit neutral hydrogen column of $N_H = 6.25 \times 10^{20}$ cm^{-2}, which is consistent with $E(B-V) = 0.13$, assuming a standard conversion (Savage & Mathis 1979, and references therein). This conversion may not be appropriate, however, since much of this extinction is probably intrinsic to the LMC. Given the (low) signal-to-noise of Lasker's data and the uncertainty of the correction, we choose instead to simply show observed relative line intensities. The UV-to-optical scaling described in § 3.2 makes an implicit correction for reddening sufficient for comparison with models.

3. DISCUSSION

3.1. *Optical Images and Comparison with X-Ray Data*

The continuum-subtracted optical images in Figure 2 show more structure to the optical emission than has been realized previously. In particular, there is considerable "knotty" emission associated with Lasker's (1978) "diffuse" disk, and the X-ray depression in the SW (highlighted by Hughes 1987) is bounded on its east side by a faint ridge of Hα emission that connects the outer disk with the inner ring. With the exception of a couple of the brightest knots on the west side, most of the knots associated with the outer disk are prominent only in Hα and [S II].

A comparison of the X-ray and optical emission line images shown in Figure 2 is very interesting. While there is a general similarity in the overall distribution of emission in the images, the relative intensities are dramatically different. Figure 5 (Plate 9) shows a contour map of the X-ray data overlaid on the Hα image from Figure 2. There are a few apparent correspondences between bright optical and X-ray knots, but there are bright X-ray knots with no apparent optical counterparts, and vice versa. In general, the optical knots that correspond to features in the X-ray data are ones that show some emission in all three of the emission-line images. The faint, linear ridge of X-ray emission in the northern part of the object (most visible in Fig. 2*d*) aligns with a faint Hα counterpart. By blinking the aligned images on an image display, one can see that the brightest portions of the outer "horseshoe" of X-ray emission tend to lie radially inside the diffuse disk as seen in the optical. The bright optical knots at the positions observed with *IUE* do not show particularly good correspondence with features in the X-ray map.

3.2. *Comparison with E0102 and with Optical Data*

The other O-rich SNR with a reasonable UV spectrum available is the SMC object E0102 (Blair et al. 1989). It is somewhat smaller and less luminous in X-rays, but shows a similar ring of high-velocity oxygen filaments (Dopita et al. 1981). Its optical spectrum is quite similar to that of N132D, so that Dopita & Tuohy (1984) derive the same temperature (23,000 K) and density (< 100 cm^{-3}) limits for both remnants. Although many of the same emission lines are seen in the UV spectrum of this object as in the spectrum of N132D, there are some striking differences as well. No He II λ1640 emission was seen in the SMC object, while N132D shows this line at both positions. No Si emission lines were seen in the SMC object, while at least one position in N132D appears to show Si. Emission from [Ne IV] λ2425 is considerably stronger in E0102 than in N132D. The C II] λ2326 line, which is one of the strongest lines in the N132D spectra, is not detected in the SMC object, E0102.

Blair et al. (1989) used combined UV/optical data on E0102 to determine that the weak UV emission relative to the optical lines, the presence of O I optical and UV recombination lines, and the large soft X-ray flux of E0102 were all consistent with X-ray *photoionization* being the dominant excitation mechanism for this object. The differences in the UV spectra

PLATE 8

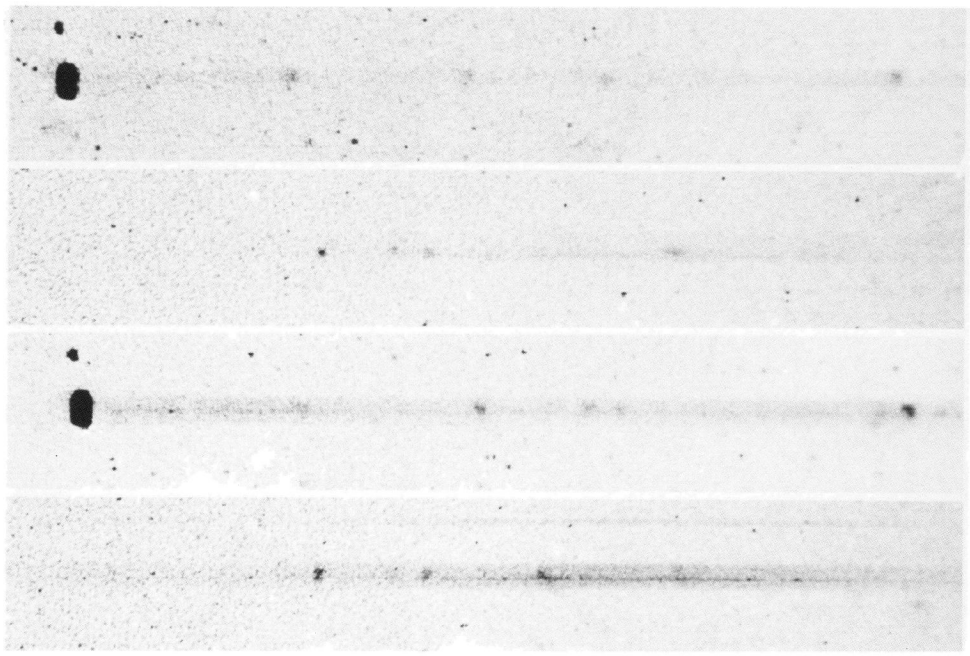

FIG. 3.—Two-dimensional *IUE* spectra for two positions in N132D. The top two panels show data for position 1, and the bottom two panels show data for position 2 (SWP on top and LWP on the bottom in each case).

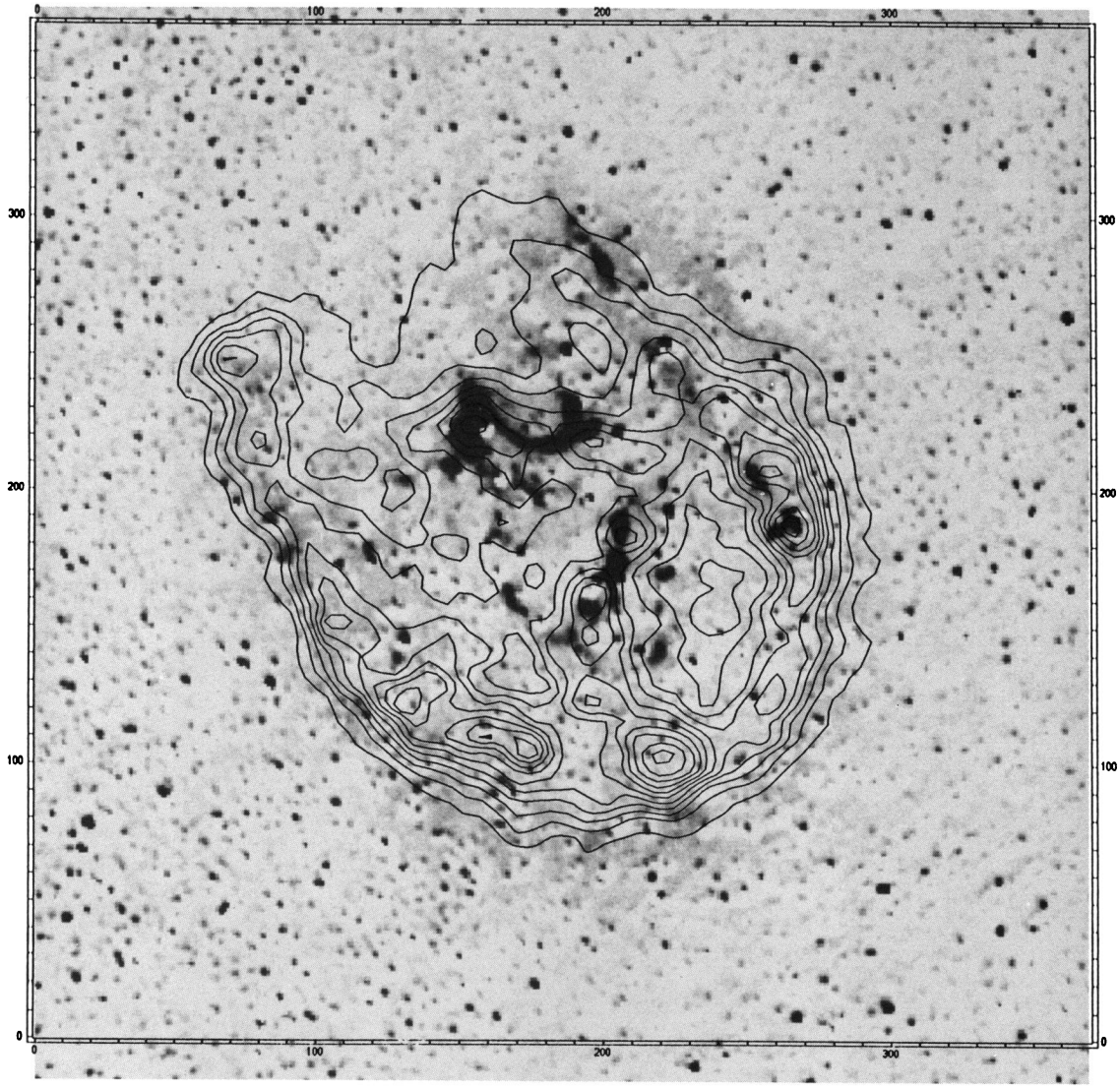

FIG. 5.—Contour map of *Einstein* HRI image of N132D aligned and projected onto the [O III] image from Fig. 2.

described above drove us (Blair et al. 1988) to a preliminary conclusion that shock heating was responsible for the emission in N132D. Here we combine optical and UV data to reexamine this preliminary result. We do not have optical data corresponding directly with the filaments observed by *IUE* in N132D, but we can at least compare the UV and optical data in a general way to test whether shock heating or X-ray photoionization is the more likely source of the observed emission. To do this, we will use the average of the two *IUE* positions and use the global optical spectrum of the O-rich knots of N132D from Dopita & Tuohy (1984). To scale these data sets, we have used the [O II] λ7320 and [O II] λ2470 lines, which come from the same upper level ($2p^2\,{}^2P$). The flux ratio of λ7320:λ2470 is given by their relative radiative transition probabilities, which is 0.78 (Mendoza 1983). This prediction should be good to 10%, which is better than the flux measurements of the lines. By way of comparison, the UV/optical scaling for E0102 was accomplished using O I recombination lines; it is comforting that the λ7320:λ2470 ratio derived for E0102 agrees to within 17% with the above prediction, which is easily within the measurement uncertainty.

The scaling of UV and optical lines to the [O II] ratio not only removes differences due to the different sizes and shapes of the *IUE* and optical apertures, but also provides a first-order correction for reddening effects. Differential reddening for lines away from these two wavelengths within the separate UV and optical wavelength bands could be sizable if the reddening is large, but as described in § 2, the reddening is thought to be fairly small. Table 3 summarizes the scaled UV and optical data, where we show the lines relative to [O III] λ5007 + λ4959 = 100.

The scaled UV and optical data show a general similarity between N132D and E0102 in that the UV lines are quite faint relative to the bright optical lines. This is one of the main facts that drove Blair et al. (1989) toward photoionized models for E0102; shock models tend to predict intrinsic UV/optical line intensities that are comparable (Itoh 1981, 1986; Dopita, Binette, & Tuohy 1984). This is unavoidable in that temperatures on the order of 10^5 K are required to collisionally ionize carbon and oxygen to the observed C^{3+} and O^{3+} states, and a temperature this high produces strong UV radiation, as well as strong [O III] λ4363 and [O II] λ7325 lines. The strong O I recombination lines in E0102 provided the other observational motivation behind the photoionization models, and those are absent in N132D. These lines arise in the densest, lowest temperature gas in the Blair et al. (1989) models, and their absence in N132D can be interpreted as a lower limit on the ionization parameter of the gas. On the other hand, the C II] and [Ne IV] lines suggest a lower ionization state in N132D than in E0102. The relative abundances of C, O, and Ne in the two remnants seem generally similar, but He and Si must be much more abundant in N132D. The temperatures implied by the ratios $I(\lambda1665):I(\lambda5007)$, $I(\lambda7325):I(\lambda3727)$, and $I(\lambda4363):I(\lambda5007)$ are all about 24,000 K.

3.3. *Comparison with Models*

The optical and UV emission from oxygen-rich SNRs is attributed generally to either radiative shock waves where dense clumps of supernova ejecta encounter the reverse shock (e.g., Itoh 1981; Dopita et al. 1984; Borkowski, Shull, & McKee 1989; Borkowski & Shull 1990) or photoionized ejecta in equilibrium or in transient ionization (Dopita 1987; Blair et al. 1989). To illustrate the differences among these models, we include one of each in Table 3 and discuss them below.

3.3.1. *Shock Model*

The shock model was computed with the current version of the Raymond (1979) shock code. It is quite similar to the original shock models for pure oxygen SNRs by Itoh (1981, 1986), the pure oxygen shocks models of Borkowski & Shull (1990) with and without thermal conduction, and the similar models for a mixture of elements in the ejecta (Dopita et al. 1984). Our model assumes elemental abundances He:C:O:Ne:Mg:Si:S in the ratios 0.001:0.3:1.0:0.3:0.3:0.1:0.03:0.01. The shock velocity and preshock temperature were taken to be 100 km s^{-1} and 1 cm^{-3}, and it was assumed that only Coulomb collisions act to transfer thermal energy from the ions to the electrons. The

TABLE 3

COMPARISON OF OBSERVATIONS[a] AND MODELS[b]

Ion	λ	N132D (LMC)	E0102−7219 (SMC)	Shock Model	Equilibrium Photoionization Model	Transient Photoionization Model
O I]	1356	<2.	15.	0.005	1.	1.
O IV] + Si IV	1400	10.9	24.	92.	8.	14.
C IV	1550	17.7	39.	37.	21.	18.
He II	1640	5.2	<2.	0.0	9.	0.0
O III]	1665	8.9	6.3	42.	4.	13.
Si III]	1885	3.0	<1.	12.	1.	1.
C III]	1907	12.5	9.0	133.	10.	43.
C II]	2325	18.4	<4.0	8.3	8.	64.
[Ne IV]	2420	6.1	13.7	0.0	9.	13.
[O II]	2470	6.0	4.4	4.2	1.	2.
Mg II	2800	3.3	4.8	3.6	21.	50.
[O II]	3727	153.	123.	75.	156.	45.
[Ne III]	3869+3968	8.9	20.	14.	21.	21.
[O III]	4363	3.3	3.6	6.5	1.	4.4
[O III]	4959+5007	100.	100.	100.	100.	100.
[O I]	6300+6363	11.	4.7	0.003	3.	1.
[O II]	7320+7330	7.8	6.8	5.6	1.	3.
O I	7774	...	2.4	0.001	2.	0.

[a] Optical observations from Dopita & Tuohy 1984. Scaling of relative optical and UV line intensities is described in the text.
[b] See § 3 for details of model calculations.

calculation was truncated when the gas had cooled to 500 K. The cooling rate is so great with this set of abundances that the gas is unable to recombine before it cools this far. Without the artificial truncation, continued recombination would enhance the O I lines at 7774 Å and 1356 Å, well beyond their observed values—a problem pointed out by Itoh (1986). We do not include a photoionization precursor because the extent of any such precursor will depend on the size of a typical knot and the time since it encountered the reverse shock, and therefore involves additional free parameters. Rather, we consider photoionized gas separately (below).

The electron temperature is nearly constant through the cooling zone, because collisional heating by electrons balances radiative losses, in agreement with the models of Itoh and Dopita et al. This region produces strong [O III] optical emission, but the 10^5 K temperature produces far too much O III] λ1665 and [O III] λ4363 emission. Our model predicts essentially no He II λ1640 emission, and even if the helium abundance is increased to equal the oxygen abundance, little He II emission is produced because [O III] excitation is so efficient compared with recombination. Models with high He abundances require higher shock velocities to produce similar spectra because of their smaller mean atomic weight.

The models described above, as well as those of Itoh (1986) and Dopita et al. (1984) assume that thermal conduction is negligible, as might be expected if the magnetic field is largely perpendicular to the flow direction (cf. discussion in Borkowski et al. 1989). Borkowski & Shull (1990) have computed models of shocks in pure oxygen assuming no magnetic suppression of thermal conduction. The enormous cooling rates of enriched gas lead to steep temperature gradients and large conductive fluxes. Their models with and without conduction both show the main characteristic of the other models; an extended plateau in which T_e is determined by the balance between heating by Coulomb collisions and cooling by excitation of oxygen ions and is typically 10^5 K. Their models without conduction predict a high T_e just behind the shock, and one effect of conduction is to remove the high T_e postshock peak. At velocities near 150 km s^{-1}, this prevents the ionization of oxygen to states above O^{2+} and greatly increases the [O III] luminosity. Our models which assumed very inefficient electron heating in the shock itself predict the same effect and differ little from the Borkowski & Shull models in the plateau region.

The second region affected by conduction is the sharp temperature drop at the end of the plateau. Here, Borkowski & Shull find a substantial conductive flux which apparently leads to strong [O III] emission from somewhat lower temperatures. While this makes the models resemble the observed spectra somewhat better, it only reduces the discrepancy in the $I(1665)/I(5007)$ ratio from about a factor of 5 to about a factor of 3. Hence, these models suffer from the same general problem as the models without conduction, which is that the UV lines are too weak in comparison with the optical line intensities. While inclusion of other effects, such as charge exchange, may eventually alter this picture, we turn next to a discussion of photoionization processes.

3.3.2. *Equilibrium Photoionization Models*

In this section, we consider equilibrium X-ray photoionization models similar to those computed by Blair et al. (1989) for E0102. The X-ray spectrum of N132D is better known than that of E0102. Clark et al. (1982) show the SSS spectrum and Hughes (1987) has described the overall spectrum and the X-ray morphology. Canizares (1990) and Hwang et al. (1992, 1993) discuss *Einstein* FPCS observations which show that the O VIII Lyα line alone accounts for 10% of the observed X-rays. To simulate the X-ray spectrum, we add the emission of carbon at 10^6 K to that of oxygen at $10^{6.4}$ K, and neon at $10^{6.6}$ K with relative abundances 1:3:1 (assuming ionization equilibrium). These temperatures are chosen to provide roughly equal emission from the H-like and He-like ion of each element and a 10:1 photon flux ratio of oxygen to neon. The actual temperature is likely to be somewhat higher (see Hughes 1987; Hwang et al. 1993), but the model we use produces relative line fluxes reasonably similar to those expected in a nonequilibrium model. Carbon is not well constrained by the X-ray observations, so we assume a proportion similar to that suggested by the UV data. The X-ray flux is scaled to the average flux implied by a luminosity of 8×10^{37} ergs s^{-1} (Hughes 1987), which for a radius of 11 pc is 6×10^{-3} ergs cm^{-2} s^{-1}. This is about half the flux employed for the E0102 models (Blair et al. 1989) due to the larger radius of N132D.

As in the E0102 models, Auger ionization is important, recombination to excited levels is included, and the charge transfer process

$$O + O^{++} \rightarrow 2\,O^{+}$$

is taken into account. We take a similar abundance set to that used in the shock model, but we assume helium and silicon abundances half that of oxygen. Because of their low temperatures, the photoionization models predict strong He II λ1640 emission.

A grid of photoionization equilibrium models was computed for comparison with the average UV/optical spectrum for N132D discussed above. Given the ionizing flux and a density, the code iterates to find thermal and ionization balance. As before, we find a strong increase in the ionization state and temperature with decreasing density. For comparison with the observations we have added the contributions of zones of oxygen densities 1.7, 1.0, and 0.3 cm^{-3} contributing 20%, 50%, and 30%, respectively, of the [O III] flux. The model temperatures are 2950 K, 6690 K, and 23,600 K, so they span most of the range covered by the models of Blair et al. (1989). The low-temperature zone dominates the [O I] emission. Higher density, lower temperature gas tends to produce too strong an O I recombination line. The middle zone dominates the [O II] emission, while the high-temperature zone supplies nearly all the ultraviolet carbon and oxygen lines.

The equilibrium photoionization models encounter the same problem in matching the data encountered by Blair et al. (1989) for E0102 and by Dopita (1987): The temperature indicated by each emission line ratio ($I(4363)/I(5007)$, $I(7325)/I(3727)$, and $I(1662)/I(5007)$) is too small. An average temperature near 24,000 K is required, but gas at that temperature in ionization equilibrium contains mostly O^{3+}.

3.3.3. *Transient Ionization*

Finally, we consider transient ionization, which has the potential for raising the gas temperature quickly enough that neutral and singly ionized material may be found at the necessary temperatures. Blair et al. (1989) considered ejecta exposed to gradually increasing X-ray flux as the reverse shock lights up the SNR as a whole, while Dopita (1987), inspired by the short lifetime of knots in Cas A (van den Bergh & Kamper 1985), considered the ionization precursor formed when an individual parcel of gas encounters the reverse shock. Neither

of these models predicts temperatures quite high enough to match the observed line ratios, but Dopita (1987) suggests that dropping the assumption of equal electron and ion temperatures would help since all the heating would go into the electrons. Blair et al. (1989) suggest consideration of the non-Maxwellian velocity distribution. Most of the heat injected by X-ray photoionization of enriched gas starts as Auger electrons ejected after K shell photoionization of C, O, or Ne. The electron energies are hundreds of eV, and they may lose this energy by exciting or ionizing the atoms or ions in the gas directly, rather than sharing it with the rest of the electrons (Shull 1979; Shull & van Steenberg 1985). The excitations produced in this process for a pure oxygen plasma have been modeled by Victor, Raymond, & Fox (1989), and it seems to make an important difference only in largely neutral gas, where it affects the O I and O II lines. Only a few percent of the energy deposited in singly or doubly ionized gas goes directly into excitation or ionization of the ions, and this affects mostly the permitted lines shortward of the *IUE* spectral range.

The model shown in Table 3 was constructed by turning on an X-ray flux of 0.39 ergs cm^{-2} s^{-1} per oxygen atom, assuming the X-ray spectrum described above. It was assumed that all the energy deposited by photoionization heats the electrons, and that only Coulomb collisions act to transfer energy to the ions. The abundance set is that used for the equilibrium photoionization models. The particular choice of ionizing flux per atom gives a reasonable ratio of UV to optical lines, in particular the O III] λ1665 line relative to λ5007. Its major failures are a lack of He II emission (in spite of a high helium abundance) and its weak [O I] and [O II] lines. Its strengths are reasonable temperature-sensitive line ratios of O II and O III, as well as the UV fluxes. It is also important to note that the model presented in Table 3 is very sensitive to the choice of ionization parameter. A 50% increase (or decrease) in the ionization parameter increases (or decreases) the ratio of UV to optical lines by about 50%.

3.3.4. *Model Summary and Discussion*

While photoionization is implicated by the relatively weak UV line emission, none of the models does an adequate job of matching the observations. A shock model which generates O III and O IV does so at temperatures which imply far too much emission in lines of [O II] $\lambda\lambda$2470, 7325 and [O III] $\lambda\lambda$4363, 1665. One might match the observations with an extremely slow shock in gas which has been photoionized by ambient X-rays. A 30 km s^{-1} shock in gas which had been X-ray ionized to O II and O III could match many of the line ratios. However, the density of the preshock gas would have to be low in that case, so that a much larger shock velocity would be predicted by equating the shock ram pressure to the pressure of the X-ray emitting shell. An equilibrium photoionization model has the opposite difficulty: While a mix of gas at different ionization parameters can match the $I(6300):I(3727):I(5007)$ ratios quite well, the temperatures are generally much too low to match the temperature-sensitive line ratios or the UV emission lines. A transient photoionization model can be chosen which does a good job with the temperature-sensitive line ratios and the UV to optical ratios, but it predicts very little [O I] and too little [O II].

It is possible that a mixture of shocks with equilibrium and transient photoionized gas can account for the observed line ratios. The drawback of this hypothesis is the striking similarity of the relative O I, O II, and O III intensities and the temperatures indicated by the optical and UV line ratios in N132D and E0102. Apparently the mix of shock parameters and ionization parameters must be very similar, though the O I], C II], and [Ne IV] intensities indicate differences at both the high- and low-ionization ends, and the strong He line in N132D suggests the presence of enough helium to strongly affect the cooling and photoionization heating rates.

A second problem is the total luminosity. The equilibrium photoionization models show that the 24,000 K gas must be at a very low density if it is ionized by the average X-ray flux alone. The very low density and high [O III] luminosity (in comparison with E0102) mean that a volume larger than that of the SNR would be needed to match the observed luminosity. Thus, if equilibrium photoionized gas contributes significantly to the total optical emission, it must be exposed to an ionizing flux many times greater than the average X-ray flux assumed in the models. This is at odds with the observed poor correlation between the X-ray and optical images, which seems to indicate that the optical knots can be ionized by the average X-ray flux.

The transient ionization models also encounter problems with the luminosity. Dopita's (1987) models predict considerable surface brightness, but they also require a large flux of oxygen atoms. Our O III] measurements, combined with the optical to UV scaling used in Table 3, imply an [O III] λ5007 luminosity of 3×10^{35} ergs s^{-1}. Dopita's models produce [O III] fluxes near 0.1 ergs cm^{-2} s^{-1} from particle fluxes of $2–3 \times 10^{10}$ O atoms cm^2 s^{-1} through the photoionization precursor. Thus these models require fluxes of roughly 0.03 $M_\odot$ yr^{-1} through the shock precursors to match the observed luminosities. Again, the poor X-ray–optical positional correlation is at odds with this model. A further possible difficulty with the transient ionization models is that they require fairly high density material to produce the observed luminosity, but high-density material exposed to the average X-ray flux would produce strong O I $\lambda\lambda$7774, 1356 lines which are not observed. For example, a solar mass of oxygen at a density of about 10 cm^{-3} would produce $L_{7774} = 10^{35}$ ergs s^{-1}, or about a third the observed [O III] λ5007 luminosity, many times the upper limit indicated by Dopita & Tuohy's (1984) nondetection.

3.4. *Abundances and Abundance Variations*

The failure of the theoretical models to adequately account for the observed spectra makes abundance determination uncertain. Nevertheless, here we make first-order estimates of abundances by number using lines of similar ionization, which should be of sufficient accuracy to be interesting in comparison with models. The abundances derived below are summarized in Table 4, along with those for the "best-fit" model of Hwang et al. (1993) for comparison. (Hwang et al.'s abundances have been scaled relative to oxygen for this comparison.)

The [Ne III]:[O III] ratio is relatively insensitive to the model, and the observed intensity ratio implies an abundance ratio somewhat smaller than was assumed in the models; Ne:O = 0.13–0.20. This is somewhat higher than claimed by Hwang et al. (1993) from the *Einstein* data; they conclude that Ne:O is 0.5–1.0 times solar (where Allen's 1973 abundances have been assumed), or 0.065–0.13 by number. (We note, however, that their best-fit model yields Ne:O = 0.14, which is consistent with our range.) The carbon abundance is crucial and is one of the important elements provided by the UV. It is probably best estimated from the C III]:O III] ratio and is predicted to be between 2.5 and 3.3 in the models, while the observed value is 1.4. Thus we find a C:O ratio of 0.13–0.17.

TABLE 4

N132D ABUNDANCES BY NUMBER RELATIVE TO OXYGEN COMPARED WITH MODELS[a]

Element	This Paper	Hwang et al.[b]	13 $M_\odot$	15 $M_\odot$	20 $M_\odot$	25 $M_\odot$
He	0.15	...	...	...	...	...
C	0.13–0.17	...	0.37	0.26	0.10	0.067
N	<0.03	...	...	...	...	...
O	1.0	1.0	1.0	1.0	1.0	
Ne	0.13–0.20	0.14	0.10	0.072	0.14	0.17
Mg	0.02	0.049	0.37	0.071	0.081	0.049
Si	0.05	0.014	0.12	0.094	0.037	0.022
S	<0.03	0.047	0.060	0.026	0.008	0.007

[a] Models are from Table 10 of Thielemann et al. (1991), after conversion to abundance by number, scaled relative to the oxygen abundance.

[b] Abundances from Hwang et al.'s (1993) "best fit" model to the *Einstein* SSS and IPC data, from their Table 2 (converted to the units of this table). Note that in their final analysis, Hwang et al. claim Ne:O = 0.5–1.0 times solar, or 0.065–0.13 by number, which is lower than the best-fit SSS/IPC model.

(Note, however, that the ratios of C IV and C II] lines to oxygen lines from similar ionization states are unfortunately quite model-dependent.)

The He II emission line is also problematic in that very different predictions come from the different models. The best estimate is probably comparison of He II λ1640:O IV] λ1400 (since recombination of He^{2+} and excitation of O IV] require ionization of He^{+} and O^{2+} whose ionization potentials are both 54 eV). If we take the $T = 23{,}600$ K photoionization model, which reproduces the temperature-sensitive line ratios, we would require 280 times more helium, or He:O = 90. It seems more likely that the helium line comes from a lower temperature region having a much higher recombination rate. The equilibrium photoionization model would suggest a He:O ratio of about 0.15.

Silicon is also uncertain, but the models generally predict Si III]:C III] ratios several times smaller than observed, so Si:C must be roughly 0.3 for the average spectrum, but positions 1 and 2 differ by at least a factor of 2. This implies Si:O $\sim$ 0.05, consistent with the solar ratio but several times larger than found by Hwang et al. (1993). The Mg II flux is also fairly model-dependent, even relative to the C II] line. It seems, however, that the assumed Mg:C ratio of 0.3 is too large, and a ratio of 0.1 or less would provide a better match. This is somewhat lower than Hwang et al.'s estimate. Upper limits on N III] λ1750 and [S II] $\lambda\lambda$6717, 6730 suggest abundances relative to O below about 0.03 at the observed positions.

These abundances can be compared with stellar evolution and nucleosynthesis calculations to derive an estimate of the mass of the precursor star of N132D (cf. Blair et al. 1984). Models of massive stars including both pre- and post-SN nucleosynthesis (Weaver & Woosley 1980; Woosley, Axelrod, & Weaver 1985; Woosley & Weaver 1986; Thielemann et al. 1991, and references therein) show a characteristic "onion skin" effect with zones of differing abundances as one moves inward through the star. Although complete "grids" of models are not available, Thielemann et al. (1991) derive the expected yields for stars with masses of 13 $M_\odot$, 15 $M_\odot$, 20 $M_\odot$, and 25 $M_\odot$, including the effects of explosive nucleosynthesis. These stars show systematic changes in the relative fractions of intermediate-mass elements, including especially C, O, Ne, and their burning products. In Table 4, we summarize the results of Thielemann et al.'s (1991) Table 10, after converting from mass units to "by number," and after scaling relative to the O abundance. From Table 4, we see rather encouraging consistency (although perhaps somewhat fortuitous given the uncertainties) with a precursor mass slightly below 20 $M_\odot$. This result is consistent with the conclusion of Hwang et al. (1993), although the uncertain mass of Fe ejected precluded them from claiming a particular mass for the precursor.

The simultaneous presence of He and O/Ne/Si/Mg in the ejecta is significant and unique in O-rich SNRs observed to date, presumably indicative of mixing at a substantial level. Massive star models indicate that He is restricted to the outer layers of the star while O and its burning products dominate interior, intermediate mass layers. Hence, mixing of these layers has apparently occurred in N132D, complicating interpretation of even our crude abundance analysis.

Clearly a more definitive knowledge of the excitation mechanisms and abundances in objects such as N132D is important for testing nucleosynthesis. In particular, the relatively large and monotonic decrease in fractional carbon abundance relative to oxygen as the precursor mass increases (see Table 4) offers great potential for pinning down the mass of the precursor star. Also, a better idea of the He:C ratio could be an important diagnostic, as it is for the Crab Nebula (cf. Blair et al. 1992; Nomoto et al. 1982).

Careful inspection of the optical images at the *IUE* aperture positions indicates that some of this mixing is due to blending of emission with different optical characteristics within the *IUE* large aperture. *IUE* has a nominal spatial resolution of $\sim$3″, but the low signal-to-noise of our long exposures prevents us from extracting information even on this relatively crude spatial scale (3″ $\sim$ 0.75 pc at 50 kpc). In particular, *IUE* position 1 clearly contains a knot dominated by [O III] emission and one bright in Hα and [S II] (with some [O III] emission) separated by about 3″, but no significant spatial variations can be derived from the *IUE* spectrum. Imaging Fabry-Perot data on N132D (J. Morse, private communication) shows a very complex velocity structure in this region, indicating that several different knots are contributing along the line of sight. Less extreme variations of velocity or relative optical line intensities are seen at *IUE* position 2, and yet the UV line intensities may vary. High spatial resolution optical and UV imaging and spectra of individual knots in N132D, which could be obtained with the *Hubble Space Telescope*, are needed to clarify the emission chacteristics of individual knots and address the extent of mixing in the ejecta.

4. SUMMARY AND CONCLUSIONS

We have presented UV spectroscopy and optical images of the oxygen-rich supernova remnant N132D in the Large Magellanic Cloud and compared with published X-ray and optical data. Although a fit of these data to a unique model has eluded us, we find broad consistency with X-ray photoionization models (as opposed to shock models) of the excitation. This is similar to what was found for E0102 in the Small Magellanic Cloud. The lack of a specific match between our models and spectra can be attributed to several causes, including blending of emission from various knots (with differing physical conditions) within the aperture or along the line of sight, or additional uncertainties in the modeling technique. Emission lines of He and probably Si have been seen in the UV spectrum of an O-rich remnant for the first time, probably indicating that mixing of the ejecta has taken place at a signifi-

cant level. Abundances have been derived from the observed line intensities, and comparison with nucleosynthesis calculations indicates a main-sequence precursor mass of about 20 $M_\odot$ for N132D.

It is a pleasure to thank the staffs of *IUE* on both sides of the Atlantic for their diligent efforts in obtaining the long exposures reported here. Also, we thank John Danziger and Roberto Gilmozzi for assisting with the *IUE* observations. We thank the staff at Las Campanas for their efforts on our behalf. Robert Kirshner provided the interference filters used for the imaging portion of this program, for which we are grateful. This work has been supported by NASA grants NAG 5-988 and NAG 5-1793 to Johns Hopkins University and NASA grants NAG 5-87 and NAGW-528 to the Smithsonian Institution.

REFERENCES

Allen, C. W. 1973, *Astrophysical Quantities* (3rd ed.; London: Athlone)
Blair, W. P., Kirshner, R. P., & Winkler, P. F. 1983, ApJ, 272, 84
Blair, W. P., Long, K. S., & Vancura, O. 1991, ApJ, 366, 384
Blair, W. P., Long, K. S., Vancura, O., Bowers, C. W., Conger, S., Davidsen, A. F., Kriss, G. A., & Henry, R. B. C. 1992, ApJ, 399, 611
Blair, W. P., Raymond, J. C., Danziger, J., & Matteucci, F. 1988, in A Decade of UV Astronomy with the *IUE* Satellite (ESA SP-281), 117
———. 1989, ApJ, 338, 812
Blair, W. P., Raymond, J. C., Fesen, R. A., & Gull, T. R. 1984, ApJ, 279, 708
Bohlin, R. C. 1986, ApJ, 308, 1001
Borkowski, K. J., & Shull, J. M. 1990, ApJ, 348, 169
Borkowski, K. J., Shull, J. M., & McKee, C. F. 1989, ApJ, 336, 979
Canizares, C. R. 1990, in IAU Coll. 115, High Resolution X-ray Spectroscopy of Cosmic Plasmas, ed. P. Gorenstein (Cambridge: Cambridge Univ. Press), 136
Chevalier, R. A., & Kirshner, R. P. 1978, ApJ, 219, 931
———. 1979, ApJ, 233, 154
Clark, D. H., Tuohy, I. R., Long, K. S., Szymkowiak, A. E., Dopita, M. A., Mathewson, D. S., & Culhane, J. L. 1982, ApJ, 255, 440
Danziger, I. J., & Dennefeld, M. 1976, ApJ, 207, 394
Dopita, M. A. 1987, Aust. J. Phys., 40, 789
Dopita, M. A., Binette, L., & Tuohy, I. R. 1984, ApJ, 282, 142
Dopita, M. A., & Tuohy, I. R. 1984, ApJ, 282, 135
Dopita, M. A., Tuohy, I. R., & Mathewson, D. S. 1981, ApJ, 248, L105
Eastman, R. G., & Kirshner, R. P. 1989, ApJ, 347, 771
Goss, W. M., Shaver, P. A., Zealey, W. J., Murdin, P., & Clark, D. H. 1979, MNRAS, 188, 357
Gunn, J. E., & Westphal, J. A. 1981, Proc. SPIE, 290, 16
Hamilton, A. J. S., Sarazin, C. L., & Chevalier, R. A. 1983, ApJS, 51, 115
Henize, K. G. 1956, ApJS, 2, 315
Hughes, J. P. 1987, ApJ, 314, 103
Hwang, U., Canizares, C. R., Markert, T. H., & Hughes, J. P. 1992, BAAS, 24, 790
Hwang, U., Hughes, J. P., Canizares, C. R., & Markert, T. H. 1993, ApJ, 414, 219
Itoh, H. 1981, PASJ, 33, 1
Itoh, H. 1986, PASJ, 38, 717
Kirshner, R. P., Morse, J. A., Winkler, P. F., & Blair, W. P. 1989, ApJ, 342, 260
Lasker, B. M. 1978, ApJ, 223, 109
———. 1980, ApJ, 237, 765
Lasker, B. M., & Golimowski, D. A. 1991, ApJ, 371, 568
Long, K. S., Blair, W. P., & Krzeminski, W. 1989, ApJ, 340, L25
Long, K. S., Dopita, M. A., & Tuohy, I. R. 1982, ApJ, 260, 202
Long, K. S., Helfand, D. J., & Grabelsky, D. A. 1981, ApJ, 248, 925
Long, K. S., Winkler, P. F., & Blair, W. P. 1992, ApJ, 395, 632
Mathewson, D. S., Dopita, M. A., Tuohy, I. R., & Ford, V. L. 1980, ApJ, 242, L73
Mathewson, D. S., Ford, V. L., Dopita, M. A., Tuohy, I. R., Long, K. S., & Helfand, D. J. 1983, ApJS, 51, 345
Mendoza, C. 1983, in IAU Symposium 103, Planetary Nebulae, ed. D. R. Fowler (Dordrecht: Reidel), 143
Murdin, P. M., & Clark, D. H. 1979, MNRAS, 189, 501
Nomoto, K., Sparks, W. M., Fesen, R. A., Gull, T. R., Miyaji, S., & Sugimoto, D. 1982, Nature, 299, 803
Raymond, J. C. 1979, ApJS, 39, 1
Raymond, J. C., & Smith, B. W. 1977, ApJS, 35, 419
Savage, B. D., & Mathis, J. 1979, ARAA, 17, 73
Shull, J. M. 1979, ApJ, 234, 761
Shull, J. M., & van Steenberg, M. E. 1985, ApJ, 298, 268
Stone, R. P. S., & Baldwin, J. A. 1983, MNRAS, 204, 347
Thielemann, F.-K., Nomoto, K., & Hashimoto, M. 1991, to appear in Supernovae, ed. J. Audouze, S. Bludman, R. Mochkovitch, & J. Zinn-Justin (Amsterdam: Elsevier)
van den Bergh, S., & Kamper, K. 1985, ApJ, 293, 537
Victor, G. A., Raymond, J. C., & Fox, J. L. 1989, International Conference on the Physics of Electronic and Atomic Collisions, 16, 402
Weaver, T. A., & Woosley, S. E. 1980, Ann. N.Y. Acad. Sci., 336, 335
Westerlund, B. E., & Mathewson, D. S. 1966, MNRAS, 131, 371
Winkler, P. F., & Kirshner, R. P. 1985, ApJ, 299, 981
Woosley, S. E., Axelrod, T. S., & Weaver, T. A. 1984, in Stellar Nucleosynthesis, ed. C. Chiosi & A. Renzini (Dordrecht: Reidel), 263
Woosley, S. E., & Weaver, T. A. 1986, ARAA, 24, 205